Trace gas measurements using optically resonant cavities and quantum cascade lasers operating at room temperature

Trace gas measurements using optically resonant cavities and quantum cascade lasers operating at room temperature

S. Welzel,[1,a] G. Lombardi,[2] P. B. Davies,[3] R. Engeln,[4] D. C. Schram,[4] and J. Röpcke[1]
[1]*INP Greifswald, 17489 Greifswald, Felix-Hausdorff-Str. 2, Germany*
[2]*CNRS LIMHP, Université Paris 13, 99, av. J.B. Clément, 93430 Villetaneuse, France*
[3]*Department of Chemistry, University of Cambridge, Lensfield Road, Cambridge CB2 1EW, United Kingdom*
[4]*Department of Applied Physics, Eindhoven University of Technology, P.O. Box 513, 5600 MB Eindhoven, The Netherlands*

(Received 7 June 2008; accepted 11 September 2008; published online 13 November 2008)

Achieving the high sensitivity necessary for trace gas detection in the midinfrared molecular fingerprint region generally requires long absorption path lengths. In addition, for wider application, especially for field measurements, compact and cryogen free spectrometers are definitely preferable. An alternative approach to conventional linear absorption spectroscopy employing multiple pass cells for achieving high sensitivity is to combine a high finesse cavity with thermoelectrically (TE) cooled quantum cascade lasers (QCLs) and detectors. We have investigated the sensitivity limits of an entirely TE cooled system equipped with an ~0.5 m long cavity having a small sample volume of 0.3 l. With this spectrometer cavity enhanced absorption spectroscopy employing a continuous wave QCL emitting at 7.66 μm yielded path lengths of 1080 m and a noise equivalent absorption of 2×10^{-7} cm^{-1} $Hz^{-1/2}$. The molecular concentration detection limit with a 20 s integration time was found to be 6×10^{8} molecules/cm^3 for N_2O and 2×10^{9} molecules/cm^3 for CH_4, which is good enough for the selective measurement of trace atmospheric constituents at 2.2 mbar. The main limiting factor for achieving even higher sensitivity, such as that found for larger volume multi pass cell spectrometers, is the residual mode noise of the cavity. On the other hand the application of TE cooled pulsed QCLs for integrated cavity output spectroscopy and cavity ring-down spectroscopy (CRDS) was found to be limited by the intrinsic frequency chirp of the laser. Consequently the accuracy and advantage of an absolute internal absorption calibration, in theory inherent for CRDS experiments, are not achievable. © *2008 American Institute of Physics*. [DOI: 10.1063/1.3008014]

I. INTRODUCTION

The development of compact and robust optical sensors for molecular detection is of interest for an increasing number of applications, such as environmental monitoring and atmospheric chemistry,[1–3] plasma diagnostics and industrial process control,[4,5] combustion studies, explosive detection, and medical diagnostics.[6–10] Absorption spectroscopy in the midinfrared (MIR) spectral region using lasers as radiation sources is an effective method for monitoring molecular species. In principle, path lengths up to several kilometers can be achieved by using optical resonators for cavity ring-down spectroscopy (CRDS), cavity enhanced absorption spectroscopy (CEAS), or integrated cavity output spectroscopy (ICOS). A wealth of studies using optical cavities were published since the introduction of CRDS by O'Keefe and Deacon in 1988,[11] of CEAS by Engeln *et al.*[12] in 1998, and of ICOS by O'Keefe and co-workers[13,14] in the same year. In CRDS the decay of light leaking out of a resonant optical cavity and provided either by a pulsed or interrupted continuous wave (cw) source is monitored in the time domain. Cavity leak-out spectroscopy (CALOS), based on cw excitation of the cavity, essentially operates on the same principle and was introduced by Mürtz *et al.*[15] in 1999. In contrast, in CEAS or ICOS the steady state transmission or integrated transmitted intensity through the cavity is observed as a function of the laser frequency. The most sensitive form so far reported is noise-immune cavity enhanced optical heterodyne molecular spectroscopy (NICE-OHMS) combining the frequency modulation technique with optical cavities.[16]

The majority of cavity based methods have used sources of radiation in the ultraviolet and visible regions. For many years the infrared spectral range could not be employed either for CRDS or for the CEAS or ICOS techniques because of the lack of suitable radiation sources with the required power and tunability, but this situation has now changed. Near infrared applications have profited from developments in telecommunications where cheap and compact light sources became available[17,18] in the 1990s, whereas similar lasers were not available in the MIR range (3–20 μm). Early experiments in the latter region were carried out with optical parametric oscillators pumped with adequately powerful lasers, e.g., in 1995 by Scherer *et al.*[19–21] The application of Raman cells or shifters was another method of choice in several studies of free radicals and stable species among them OH, CH_3, or clusters of water and CH_3I.[22–26] Peeters *et al.*[27] measured ethylene at 10 μm with a waveguide CO_2 laser in a CEAS configuration. Mürtz and co-workers[15,28,29] performed CALOS experiments with CO_2 and CO lasers to

[a]Author to whom correspondence should be addressed. Electronic mail: welzel@inp-greifswald.de.

detect C_2H_4, $^{13}CH_4$, and OCS, respectively. In all these cases sophisticated optical geometries were developed which were more suitable for the research laboratory than for field applications.

To overcome the drawbacks of the bulky radiation sources mentioned above, small semiconductor-based lasers became increasingly used. In 2001 a MIR cavity ring-down spectrometer, using lead salt lasers, was reported.[30–32] It was possible to detect CO but clearly the technique suffered from low laser intensity. Recent advances in semiconductor laser technology, in particular, the advent of intersubband quantum cascade lasers (QCLs) and interband cascade lasers (ICLs),[33–36] provides new possibilities for highly sensitive and selective trace gas detection using MIR absorption spectroscopy[1,37–44] and enabled sensitivities of 5×10^{-10} cm^{-1} $Hz^{-1/2}$ to be accomplished but at the expense of large sample volumes.[39] Distributed feedback (DFB)-QCLs combine single-frequency operation with tunability over several wavenumbers, and average powers over a milliwatt; hence they are superior to lead salt lasers. While pulsed QCLs working at room temperature have been commercially available for several years, room-temperature cw QCLs have only recently been introduced. The relatively high output power of the QCL permits the use of optical cavities with high finesse. With the help of such cavities the effective path length of the laser beam in the absorbing medium can essentially be increased to more than the 200 m limit usually available from conventional optical multipass cells[38,45] while keeping the sample and pumped volume small.

The potential of such a combination was demonstrated in CRDS measurements with a cryogenically cooled cw DFB-QCL.[46] A sensitivity of 9.7×10^{-11} cm^{-1} $Hz^{-1/2}$, i.e., within an order of magnitude of the ultimate shot-noise-limit, was achieved with the application of QCLs to NICE-OHMS.[47] Focusing on potential field-deployable systems, Silva *et al.*[8] reported a study which combined a thermoelectrically (TE) cooled pulsed QCL with CRDS and ICOS. A calibration of nonlinear experimental results was necessary and the observation of asymmetric line shapes caused by the frequency chirp in a single laser pulse was discussed. Other studies combining TE cooled pulsed QCLs with the CRDS approach recognized the influence of the frequency chirp of QCLs leading to disturbed line profiles followed by reduced sensitivity and selectivity.[48,49] Further development was forthcoming from the availability of DFB-QCLs with increasingly good performance such as output power and near ambient temperature operation, in the beginning limited to the 5–10 μm range. Several applications of QCLs combined with either the CRDS or the CEAS/ICOS techniques for trace gas detection[50–57] followed, and sensitivities down to 2×10^{-9} cm^{-1} $Hz^{-1/2}$ were reported.[51] Recently, the availability of ICL, which emits in the 3–5 μm range, also enabled ICOS experiments on H_2CO to be performed.[58] However, the broader use of cavity based techniques in the MIR in industry or for field application has so far not only been hindered by space or weight restrictions but also by the need for cryogenic cooling of either the laser or (at least) the detector. Recently there has been a trend away from liquid nitrogen (LN) cooled systems toward TE cooled devices,[54,55] but the performance of an entirely TE cooled system based on optical cavities has not yet been investigated.

TE cooled pulsed and cw QCLs have been employed for high finesse cavity absorption spectroscopy in the MIR. Our approach was twofold: (i) CRDS and ICOS experiments have been performed with pulsed QCLs and (ii) a room-temperature cw QCL was used in a complementary CEAS configuration aimed at achieving a sensitive, LN free spectrometer for sampling small volumes. In the CRDS experiment the influence of the frequency chirp of pulsed QCLs on the sensitivity and accuracy of concentration measurements has been analyzed in detail using CH_4 and N_2O as absorbing gases. Apart from several studies on NO at 5 μm the MIR spectral region in general and the 7–8 μm region presently used have not been extensively investigated.

After a short compilation of the necessary formulae for data analysis in Sec. II, the experimental arrangements for the different approaches are presented in Sec. III. Section IV follows with a detailed analysis of the CRDS and ICOS experiments with the pulsed QCLs, and the validation of the CEAS system. Finally, the conclusions are presented in Sec. V.

II. THEORETICAL CONSIDERATIONS

This section summarizes the basic equations which are necessary to analyze the recorded data. A more thorough introduction with a detailed discussion of different approaches and the assumptions lying behind the formulae which are in common use was recently published in a comprehensive review by Mazurenka *et al.*[59] The fundamental equation for a laser absorption experiment is the Beer–Lambert law. For a constant number density n along the line of sight this is expressed as

$$\ln\left(\frac{I_0(\nu)}{I(\nu)}\right) = k(\nu)L_{\text{eff}}, \tag{1}$$

where I and I_0 are the transmitted and incident intensities, respectively, L_{eff} is the effective absorption path length in the absorbing medium, and depends on which method is applied, and $k(\nu)$ is the frequency dependent absorption coefficient defined as

$$nS = n\int_{\text{line}} \sigma(\nu)d\nu = \int_{\text{line}} k(\nu)d\nu. \tag{2}$$

The integrated absorption cross section σ is usually referred to as the line strength S. Following the description of Mazurenka *et al.* only a few restrictions are used for the ballistic assumption (or ping-pong model) to describe the behavior of a laser pulse shorter than the round trip time in an optical resonator, namely, that the reflectivity of the cavity mirrors is equal ($R_1=R_2\equiv R$) and scattering is neglected, i.e., the transmission $T\approx1-R$. The separation of the highly reflective mirrors is L, whereas the interaction length of the laser beam with the absorbing medium is d. The intensity I^0 directly transmitted through the cavity without any additional round trip is then

$$I^0 = (I_{\text{in}}\eta T)e^{-kd}T, \tag{3}$$

where $\eta(\leq 1)$ factors in the possibility of nonideal mode matching of the incident radiation I_{in} with the cavity modes.[59] After m round trips the intensity leaking out of the cavity I^m is

$$I^m = I^0(Re^{-kd})^{2m}. \tag{4}$$

Although strictly speaking the ballistic assumption is only valid for short laser pulses exponential decays—according to the above mentioned treatment—can be also observed for light pulses longer than the round trip time as long as the absorption line is broader than the spacing of the evolving cavity modes.[60]

A. Cavity ring-down effect

Equation (4) can readily be transformed into the well-known relationship for the cavity ring-down intensity

$$I^m = I^0 \exp\left(-\frac{t_m}{\tau}\right), \tag{5}$$

where the decay time τ is defined by

$$\tau(\nu) = \frac{L}{c[k(\nu)d - \ln R]}, \tag{6}$$

and the time t_m necessary for a cavity round trip is given by $t_m=(2\text{mL})/c$, where c is the velocity of light. In the case of typically high values for the mirror reflectivity, $R\rightarrow 1$, Eq. (6) can be approximated by

$$\tau(\nu) \approx \frac{L}{c[(1-R) + k(\nu)d]}. \tag{7}$$

For an empty cavity ($k=0$) and with $d=L$ (absorbing medium completely filling the cavity), an effective absorption path for the experiment $L_{\text{eff}}=c\tau_0=L/(1-R)$ can be defined. Transforming Eq. (7) yields the absorption coefficient

$$n\sigma(\nu) = k(\nu) = \left(\frac{1}{\tau(\nu)} - \frac{1}{\tau_0(\nu)}\right)\frac{L}{dc}, \tag{8}$$

which can be calculated from measurements in the time domain.

B. Cavity enhanced absorption

The cw excitation of a cavity (CEAS) was originally introduced by Engeln *et al.*[12] The description of the temporal development of the intensity inside the cavity I_{cav} is similar to Eq. (4). The only difference is an additional source term taking into account the continuously available radiation rather than a short laser pulse[51]

$$\frac{dI_{\text{cav}}}{dt} = \frac{c}{2L}[I_{\text{in}}\eta T - 2I_{\text{cav}}(1 - Re^{-kd})] \tag{9}$$

leading to a steady state output of the cavity characterized by

$$I_{\text{out}}(t) = \frac{I_{\text{in}}\eta T^2}{2(1-Re^{-kd})}\left[1 - \exp\left(-\frac{t}{\tau}\right)\right]. \tag{10}$$

This is governed both in time and amplitude by the cavity losses (R and k). Hence the laser frequency sweep has to stay long enough in resonance with the cavity modes to enable a sufficient intensity buildup inside the cavity. At the same time the scan rate must be significantly higher than the jittering of the cavity modes to avoid large intensity fluctuations.[12] Using the steady state output the ratio of the intensities for an empty (I_0) and a filled (I) cavity can be defined as

$$\frac{I_0}{I} = \frac{I_{\text{out}}(k=0)}{I_{\text{out}}} = 1 + GA, \tag{11}$$

where $G=R/(1-R)$ and $A=[1-\exp(-kd)]$.[51] Eq. (11) is valid for all R and k. It is easy to show that in the weak absorption limit ($k\rightarrow 0$ and $R\rightarrow 1$) Eq. (11) becomes

$$n\sigma(\nu) = k(\nu) = \left(\frac{I_0(\nu)}{I(\nu)} - 1\right)\frac{1-R}{d}. \tag{12}$$

By analogy with Beer–Lambert law (1) assuming weak absorption the effective path length can thus be expressed as $L_{\text{eff}}=L/(1-R)$ for $d=L$.

Equation (12) can be analyzed further. If the natural logarithm is taken from Eq. (11) and plotted against the molecular number density n a linear relationship is expected, as long as a weak absorber is present in the cavity. In this case the expressions can be further simplified to

$$\ln\left(\frac{I_0}{I}\right) \approx GA \sim n. \tag{13}$$

Thus Eq. (13) fulfils two functions. First, it serves as a check on the validity of the weak absorption limit. Second, in the range where $\ln(I_0/I)$ is proportional to n, the slope of this linear relationship enables the mirror reflectivity R to be determined from a known concentration standard and hence provides a means for the absolute calibration of CEAS (or ICOS, as will be shown in Sec. II C).

C. Integrated cavity output

ICOS was introduced for pulsed excitation of the cavity.[14] For data analysis there is, in fact, no difference from CEAS since Eq. (12) holds for cw as well as for pulsed excitation. In the latter case the source term in Eq. (9) is absent after the initial excitation. On the other hand, following the ping-pong model, the integrated cavity output I_{out} corresponds to an infinite sum over the intensity I^m leaking out of the cavity,

$$I_{\text{out}} = I_{\text{in}}\eta(1-R)^2e^{-kd}\sum_{m=0}^{\infty}(Re^{-kd})^{2m}$$

$$= I_{\text{in}}\eta(1-R)^2\frac{e^{-kd}}{1-(Re^{-kd})^2}. \tag{14}$$

The sum over m converges for the experimentally reasonable cases when $R\exp(-kd)<1$ and yields the right hand side of (14). The ratio of the time integrated signal of the cavity

without $(k=0)$ and with the absorbing medium is correspondingly

$$\frac{I_0}{I} = \frac{I_{\text{out}}(k=0)}{I_{\text{out}}} = \frac{1-(Re^{-kd})^2}{(1-R^2)e^{-kd}}. \tag{15}$$

In the limits of weak absorber $(k \to 0)$ and high reflectivity $(R \to 1)$ Eq. (15) can be simplified to

$$\frac{I_0}{I} \approx 1 + \frac{kd}{1-R}, \tag{16}$$

which is the standard formula used for ICOS, leading essentially to the same result as in the CEAS case embodied in Eq. (12).

In what follows the terms ICOS and CEAS are thus used synonymously, in other words ICOS is used in the context of pulsed excitation and CEAS in the context of cw cavity excitation. In both cases Eq. (12) will be applied to extract the absorption coefficient whereas Eq. (8) is applied to the CRDS measurements.

D. Detection limits

For CRDS the uncertainty in the absorption coefficient Δk can be derived from Eq. (8) with $\tau \to \tau_0$

$$\Delta k = \frac{\Delta\tau}{\tau_o^2}\frac{L}{dc}. \tag{17}$$

Conventionally the standard deviation of the ring-down time is used as a measure of $\Delta\tau$. For CEAS and ICOS an analogous relationship can be found from Eq. (12) with $I \to I_0$,

$$\Delta k = \frac{\Delta I}{I_0}\frac{1-R}{d}, \tag{18}$$

where ΔI represents the intensity fluctuations, either inherent to the light source or induced by mode fluctuations. For practical reasons the standard deviation of the intensity fluctuations on the base line will be used here to estimate ΔI. In principle, the error in the absorption coefficient is even higher since the reflectivity of the mirrors R is not known, i.e., a calibration is required leading to a $\sqrt{2}$ times higher uncertainty in k.[59] In general, another quantity, namely, the noise equivalent absorption (NEA) defined in Refs. 19 and 59 is used to estimate the detection limit

$$\text{NEA} = \Delta k \sqrt{\frac{2}{f}}, \tag{19}$$

where f is the repetition rate of the measurements, i.e., the number of averages in a 1 s interval.

III. EXPERIMENTAL

Two different kinds of experiment are described here for both of which essentially the same optical setup was used: first conventional cavity ring-down with a pulsed light source (Sec. III A) and second CEAS using a cw QCL in order to obtain a highly sensitive LN free sensor scheme in the MIR (Sec. III B). The changes required for the cw source and the different analyses of the data will be outlined in Sec. III B. Basically, for both approaches the laser frequency was swept by a continuous current ramp. In contrast to locked cavity studies, the cavity length here was not actively changed or dithered nor was the cavity locked to the illuminating light source.

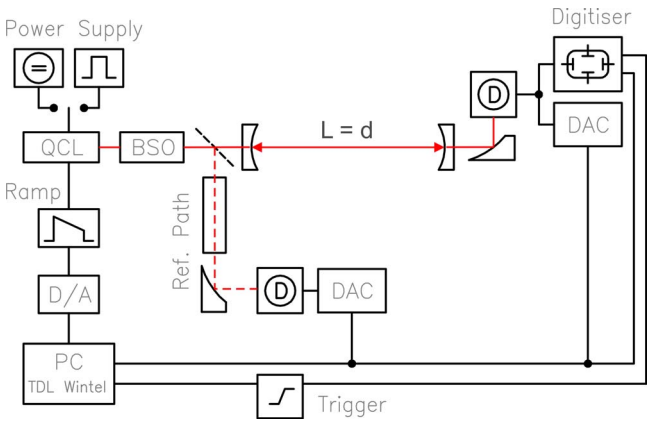

FIG. 1. (Color online) Schematic of the apparatus used for both CRDS and CEAS experiments. BSO provided efficient light transmission to the resonator. The detector (D) signals were recorded with data acquisition cards (DACs). The QCLs were driven either by a pulsed or a cw source and the tuning ramp for the laser was generated via the digital-to-analog-converter (D/A).

A. Pulsed cavity excitation

The experimental arrangement using pulsed QCLs is straightforward, as shown in Fig. 1. The stable resonator was formed by two high reflectivity mirrors (Los Gatos Research) of diameter 25.4 mm and 1 m radius of curvature. The mirrors also served to enclose the vacuum vessel which was made of standard vacuum components. Hence the vacuum cell determined the mirror separation of 0.432 m. Beam shaping optics (BSO) collected the strongly divergent radiation from the QCL first with an off-axis parabolic mirror (OAP) of 49.5 mm diameter $(f/0.99)$ and then with a telescope formed by two additional OAPs which reduced the beam diameter by a ratio of almost 1:5. This was sufficient to effectively match the 20 mm aperture of the cavity. No additional optics were added to suppress possible optical feedback to the laser, since feedback was assumed to be negligible for the current DFB-QCL devices. The radiation leaking out of the cavity was collected by an OAP of 25.4 mm diameter $(f/0.64)$ and directed to a detector and preamplifier with a response time of approximately 70 ns. For CRDS relative calibration was provided by recording the fringes of a germanium etalon in a reference channel and using interpolation. Absolute calibration was achieved by comparison with standard gas absorption spectra recorded in the reference channel simultaneously with the CRDS spectra. Typically the same stable molecule was used for calibration and cavity experiments. Both signal and reference channel were equipped with LN cooled detectors (Judson Technologies, J15 series).

The QCL was driven and frequency swept using an external trigger signal and voltage ramp (Q-MACS, neoplas control). This is frequently referred to as the *interpulse* mode, i.e., several amperes are provided by triggered current pulses superimposed on a subthreshold current ramp. The

pulses vary from a few to up to tens of nanoseconds with a duty cycle of considerably less than 5%. The current is ramped over several hundred pulses in order to sweep the laser frequency. Each laser pulse represents a spectral data point in the spectrum. A full spectrum is therefore acquired in milliseconds. Generally, the spectrum consisted of 160 points while the laser was active and 30 pulses while the laser was off, in order to obtain the offset or zero signal. The repetition frequency of the trigger was set to 10 kHz which enabled the decay transient—being of the order of less than 10 μs—to be followed completely and without any distortion. A fast digitizing oscilloscope (LeCroy, Waverunner 104Xi) was used to acquire the ring-down transients. All the decays of a single sweep (190 pulses$\times$100 μs trigger period=19 ms) were recorded with an appropriate time resolution (submicrosecond range) in one shot. In practice the ring-down decay was recorded for several microseconds and the rest of the QCL off-phase was not detected until the next trigger event occurred. In this way a data set consisting of 160 single nonaveraged decays was obtained. The ring-down transients were then processed according to Eq. (8) for CRDS and Eq. (12) for ICOS, i.e., each ring-down transient was analyzed twice, first with a linear fit to the decay on a semilogarithmic scale from which τ was obtained, and second the area under the transient decay was integrated to obtain the integrated cavity output I. The base line I_0 for ICOS required in the data in Figs. 5 and 8 was similarly determined by integrating over the output of an empty cavity.

Two pulsed QCLs (Alpes Lasers) were used for the experiments. One emitting between 1345 and 1352 cm^{-1} ($\sim$7.42 μm) almost coincided with the center wavelength of the high reflectivity mirrors, whereas the emission of the second laser between 1195 and 1200 cm^{-1} ($\sim$8.35 μm) coincided with the edge of the low loss range of the cavity mirrors. The first QCL was operated at 1.6 °C corresponding to an emission sweep from 1347.6 to 1348.2 cm^{-1}. A pulse width of 60 ns was chosen in order to inject enough power into the cavity. For the 8.35 μm laser a pulse width of 32 ns was adequate to detect a signal from the cavity. For this laser the temperature was set at 4.0 °C resulting in a spectral output of 1197.2–1197.8 cm^{-1}.

B. Continuous cavity excitation

The only difference to the optical setup in Sec. III A and Fig. 1 is that the radiation of the QCL was directed to the telescope with an aspherical ZnSe lens (30 mm diameter, f/1.5). The cw QCL (Alpes Lasers) emitted from 1300 to 1311 cm^{-1}. It was operated in a standard housing (Starter Kit, Alpes Lasers) and TE cooled to −5.9 or +2.2 °C for trace gas measurements in room air. A dc source (Kepco, BOP100–2M) provided up to 2 A and 100 V. The laser was typically driven with a dc of around 380 mA. An additional current ramp of 45 mA was impressed on it in order to sweep the laser frequency during the on-phase. The laser current was briefly reduced below the threshold value by −70 mA to record the offset of the zero signal (Fig. 2) in the off-phase. The sweep rate of the laser was 0.9 kHz for all measurements.

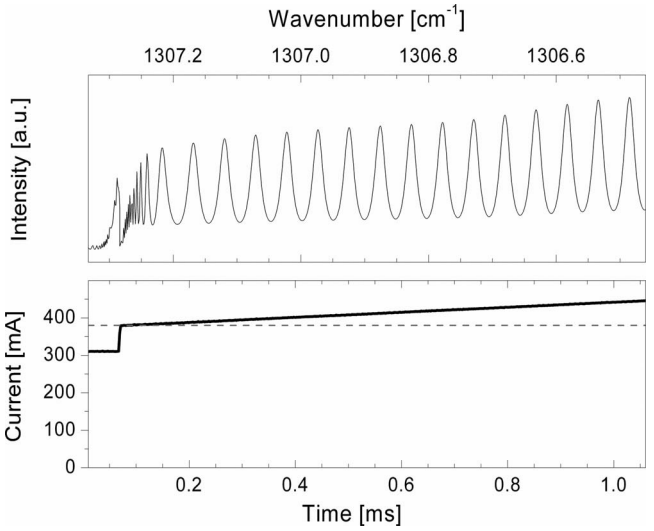

FIG. 2. Lower: Average current (dashed line) and its modulation (heavy black line) applied to the cw QCL during a single sweep. Upper: Signal through a 25.4 mm germanium etalon (0.048 cm^{-1} FSR) demonstrating the 0.78 cm^{-1} sweep of the laser when the modulation ramp was applied.

The spectra (on-phase) consisted of 800 points with an additional off-phase of 50 points. After switching the current from the off to the on-phase the QCL required a short period of about 50 μs to stabilize its temperature and therefore its frequency. After that the laser sweeps 0.78 cm^{-1} or 23.4 GHz with the current modulation applied. This is illustrated at the top of Fig. 2 showing the signal through a germanium etalon. In combination with stable reference gases (CH_4, N_2O) this scan also served for the identification and calibration of the frequency axis of the spectra. For a mirror distance of 0.432 m, used for all experiments, the sweep of the laser frequency corresponds to a scan over 67 cavity modes. In other words after approximately 14 μs a new cavity mode was excited which was sufficient to avoid an overlap between the buildup and decay events of different modes. On the other hand the sweep rate gave a full spectrum after slightly more than 1 ms. A given number of spectra were then averaged and simultaneously fitted. In order to smooth interference effects on the base line of the spectra, mainly caused by longitudinal cavity modes, the whole cavity was arbitrarily destabilized mechanically, e.g., by an external vibrating source. Averaging over 5 s or more reduced the interference fringes to below the noise level induced by all the data acquisition electronics.

First, the cavity output signal and reference spectra were recorded with the same LN cooled detectors used in the CRDS. Since the sensitivity of the fast detector, formerly sensing the ring-down transients, was lower for the current spectral range it was replaced by the detector used formerly as a reference detector. Next, a TE cooled detector (neoplas control, VIGO element PDI-3TE-10/12) was employed for the signal channel.

IV. RESULTS AND DISCUSSION

CRDS and ICOS measurements with two different pulsed QCLs are presented in Sec. IV A. The pulse length was chosen to be as short as possible while maintaining a

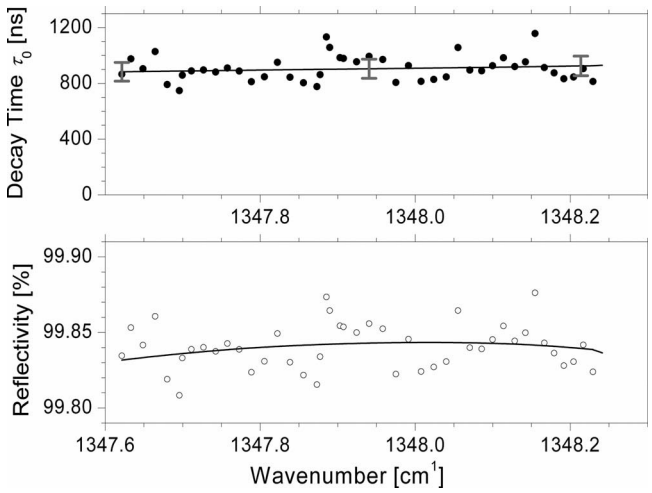

FIG. 3. Decay time measured at 7.42 μm for an empty cavity (upper) and the corresponding mirror reflectivity (lower). Solid lines represent a polynomial fit to the data.

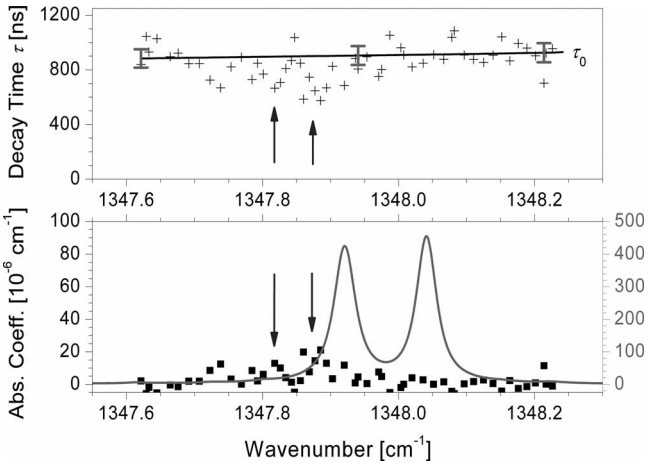

FIG. 4. CRDS results for 100 ppm CH_4 in Ar at 300 mbar total pressure: decay time τ (upper) and the corresponding absorption coefficient k (lower). Filled squares in the lower panel are the experimental absorption points; solid line is the calculated spectrum. Note the five times scale magnification for the calculation (right hand scale). Arrows in the upper and lower panel indicate potential low intensity absorption features.

reasonable cavity output. The achieved sensitivities are compared with conventional multiple pass spectrometers. The parameters which determine the sensitivity are quantitatively discussed and summarized in detail in Sec. IV B. The evaluation of a CEAS system including a discussion on current sensing limits is presented in Sec. IV C.

A. CRDS and ICOS using a pulsed QCL

1. CH_4 detection at 7.42 μm

The characteristics of the empty cavity were first established (Fig. 3). The average τ_0 across the spectral mode was 900 ns corresponding to a mirror reflectivity of about 99.84%, which was slightly lower than specified, and an effective absorption path length L_{eff} of 270 m. A relative error, $\Delta\tau/\tau_0$, of about 7.6% was estimated from the scatter of the τ_0 data. For the case of $L=d$ in Eq. (17) this corresponds to a minimum detectable (peak) absorption coefficient of 2.8×10^{-6} cm^{-1} in a single shot experiment. The theoretical NEA for the ~50 Hz laser sweep rate should be 4×10^{-7} cm^{-1} Hz$^{-1/2}$. However, in practice averaging experiments were not undertaken to achieve this theoretical figure.

When CRDS and ICOS spectra of 100 ppm CH_4 in a background of 300 mbar Ar were recorded deviations from τ_0 or I_0 were observed. For the CRDS spectrum (Fig. 4) the indicated deviations are slightly more pronounced than the scatter of the τ_0 data (Fig. 3), but nevertheless the potential absorption features hardly exceed the noise level. The experimental absorption coefficient in Fig. 4 never exceeds 2×10^{-5} cm^{-1} as shown around 1347.85–1347.90 cm^{-1}. The ICOS spectrum (Fig. 5) appears not to be as noisy as for the CRDS case (integration over the cavity output is in fact an averaging process) and the deviation from the base line I_0 (Fig. 5) is now obvious. The k values from the ICOS spectrum are below 6×10^{-5} cm^{-1}, clearly larger than that obtained from the CRDS analysis but almost a factor of 10 less than expected from a calculation using the HITRAN database (2004 edition).[61] The two CH_4 lines that should theoretically appear in the spectra under the current conditions are indicated in Figs. 4 and 5. Both should be clearly resolved and exhibit an absorption coefficient of nearly 5×10^{-4} cm^{-1}. Hence the shortfall in k of the CRDS results is a factor of 25 or greater. On the other hand the features in Fig. 4 and especially Fig. 5 suggest broadband absorption, i.e., unresolved absorption of several lines, rather than single CH_4 lines. This potential broad absorption feature appears well below the reference position of one of the single CH_4 lines at 1347.92 cm^{-1}, which has been carefully calibrated with the peak of the corresponding CH_4 feature in a reference cell.

Similar observations were made by Sukhorukov *et al.*[49] They concluded that the dual effects of line broadening and line position shifts might be minimized to some extent by reducing the pulse widths used to operate the laser. In our case it is 60 ns and it was found that reducing it lead to an insufficient signal for detection after the cavity.

2. N_2O detection at 8.35 μm

Since smaller QCL pulse widths might improve the sensitivity and selectivity of the pulsed CRDS experiments, it

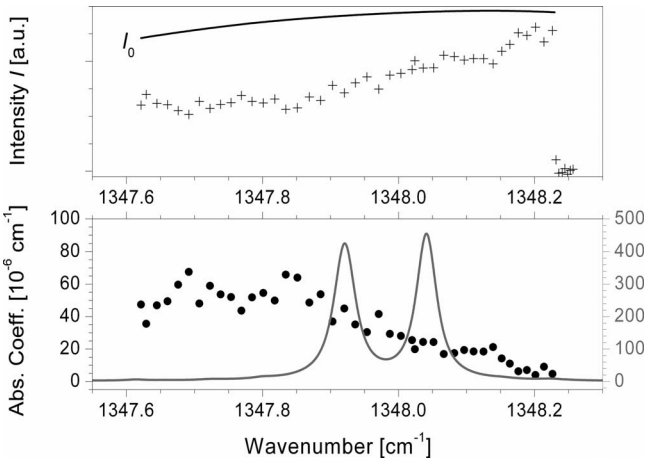

FIG. 5. ICOS results for 100 ppm CH_4 in Ar at 300 mbar total pressure: the absorption coefficient k (lower) was derived from I_0/I values in the upper spectrum. Filled circles in the lower panel are experimental absorption points, solid line is the calculated spectrum. Note the five times scale magnification for the calculation (right hand scale).

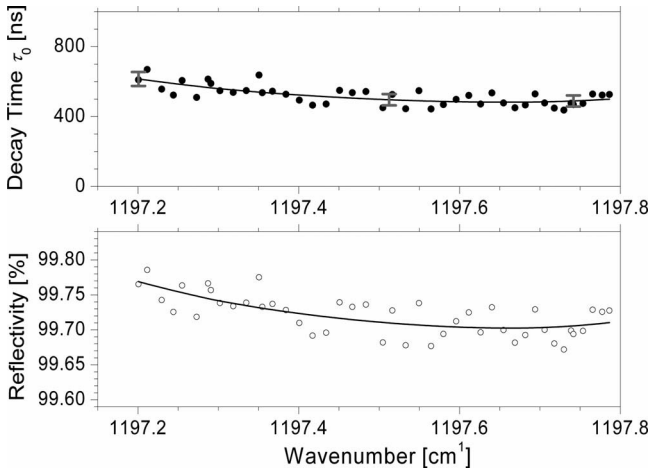

FIG. 6. Decay time measured at 8.35 μm for an empty cavity (upper) and the corresponding mirror reflectivity (lower). Solid lines represent polynomial fits to the data.

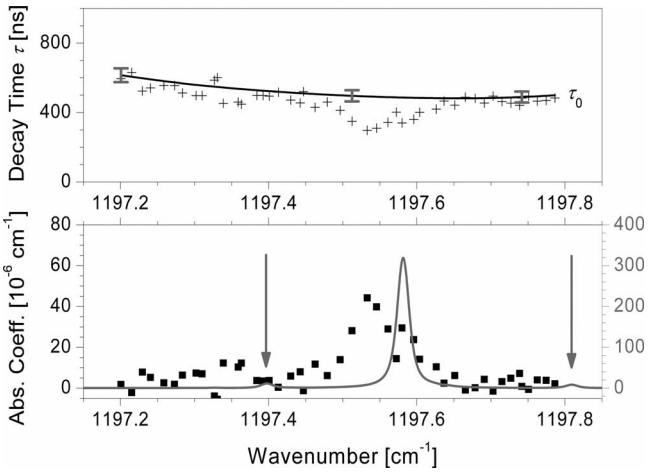

FIG. 7. CRDS results for 1667 ppm N_2O in N_2 at 100 mbar total pressure: decay time τ (upper) and the corresponding absorption coefficient k (lower). Filled squares in the lower panel are the experimental absorption points; solid line is the calculated spectrum. The arrows indicate two weak N_2O absorptions in the calculated spectrum. Note the five times scale magnification for the calculation (right hand scale).

was decided to move to the 8.35 μm region where the mirror reflectivity is lower (transmission >0.16%). A pulsed QCL emitting at the edge of the high reflectance regime of the same mirror set was combined with the cavity. This enabled the laser pulse width to be reduced to 32 ns. The decay time of the empty cavity was ~500 ns corresponding to an expected drop in the reflectivity to 99.71% (Fig. 6), i.e., almost quadrupling the intensity transmitted through one mirror. The effective path length L_{eff} falls to 150 m which is now of the same order of magnitude as available from the conventional Herriott-type long path cells. The relative error in $\tau \sim 6.5\%$ is similar to that reported above for CH_4. For a single shot experiment the minimum detectable (peak) absorption coefficient is $\sim 4.3 \times 10^{-6}$ cm^{-1}, reduced due to the absorption length. The corresponding NEA in the case of averaging would be 6.1×10^{-7} cm^{-1} Hz$^{-1/2}$.

Next, measurements were performed with a gas mixture consisting of 1667 ppm N_2O in N_2 at a pressure of 100 mbar. Some improvements in the CRDS spectra (Fig. 7) as well as in the ICOS spectra (Fig. 8) can be detected compared to the previous CH_4 experiments. The spectra exhibit an absorption line but artifacts similar to those described above are still present. An N_2O absorption feature is indicated by an unambiguous drop in the decay. The peak absorption coefficient k derived from CRDS is about 5×10^{-5} at 1197.5 cm^{-1}. Nevertheless the data points in the spectrum are still fairly scattered. Notably the ICOS spectrum shows a significant improvement compared to all other spectra presented earlier. The absorption coefficient is of the same order of magnitude as deduced from the CRDS experiments. The peak appears at 1197.58 cm^{-1} (Fig. 8) and the broadening mentioned earlier shows up as a shoulder to the left of the absorption line. Although this result is qualitatively closer to the calculated frequency from the HITRAN database, it still falls short by at least a factor of 8 in the absorption coefficient.

3. Sensitivity conclusions

It could be argued that both the CH_4 and the N_2O absorption features chosen as examples are far too strong for a standardization test since saturation effects could arise thereby reducing the experimental absorption coefficients. In this case weaker absorption features would show a better agreement between experiment and calculation. However, considering e.g., the smaller N_2O lines which should appear at 1197.40 and 1197.81 cm^{-1} (Figs. 7 and 8, respectively) it is clear that potential saturation effects cannot explain the observed effects. The small N_2O line at 1197.40 cm^{-1} appears above the noise level and agrees with the calculation, but note that the latter is plotted with a ×5 scale magnification. The shortfall in k for weaker or stronger lines is very similar, i.e., the sensitivity is systematically limited.

If we assume that spectral averaging was carried out the achieved sensitivity for the pulsed CRDS measurements should be either 4×10^{-7} cm^{-1} Hz$^{-1/2}$ (7.42 μm) or 6×10^{-7} cm^{-1} Hz$^{-1/2}$ (8.35 μm). These values are approximately a factor of 10 better than estimated from similar ex-

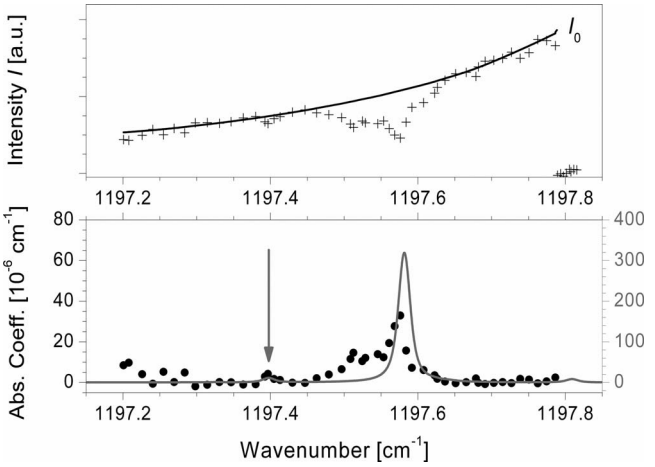

FIG. 8. ICOS results for 1667 ppm N_2O in N_2 at 100 mbar total pressure: the absorption coefficient k (lower) was derived from I_0/I values in the upper spectrum. Filled circles in the lower panel are experimental absorption points, solid line is the calculated spectrum. The arrow indicates a weak N_2O absorption which is also visible in the experimental spectrum. Note the five times scale magnification for the calculation (right hand scale).

periments performed by Manne *et al.*[48,62] and a factor of 10 worse than ICOS results with a pulsed TE cooled QCL.[8,63] In the latter case a better signal-to-noise ratio (SNR) and an approximately five times longer effective path length yielded better sensitivity. For CRDS with a cw QCL a notably higher sensitivity was reported [4×10^{-9} cm^{-1} $Hz^{-1/2}$ (Ref. 46)] also suggesting a systematic source of error with pulsed QCLs. It is interesting and instructive to compare the NEA of the different CRDS measurements with that using a long path cell. For comparison, Menzel *et al.* used a Herriott cell type QCL spectrometer of path length 100 m. Their NEA for short time measurements (~1 s) is estimated to be 3×10^{-8} cm^{-1} $Hz^{-1/2}$ (Refs. 50 and 64) and would therefore be superior to the high finesse cavity setup used here. More recently Nelson *et al.*[38] improved the detection limit for a Herriott cell (210 m) combined with a QCL to 3×10^{-10} cm^{-1} $Hz^{-1/2}$,[65] i.e., about three orders of magnitude better than employing resonant optical cavities with pulsed QCLs and still an order magnitude better than with cw QCLs as the laser source.

To summarize, the main obstacles in the experiments with a pulsed QCL combined with a high finesse optical resonator are: the selectivity is decreased due to arbitrarily broadened and shifted absorption lines and the sensitivity is substantially reduced due to diminished absorption signals in comparison with theory. Clearly, this could be overcome by calibration[48,49] but in doing so, one of the major advantages of CRDS, namely, the calibration free measurement approach, is lost. Conversely this raises the question as to whether the combination of an optical cavity with a pulsed QCL in order to benefit from reduced sample volumes compared to multiple pass cells of the same effective length is desirable as a calibration free method. The reason for these degradations from the theoretical performance should be accounted for because the measurements of τ_0 with empty cavities show potential for obtaining quantitative results.

B. Bandwidth effects with a pulsed QCL

Possible explanations for the effects observed here can be found in the work of Sukhorukov *et al.*[49] They discussed the deviations in their measurement series (i.e., absorption lines with an increased linewidth and shifted line positions with increasing pulse width), which were not as pronounced as those presented here, in terms of the well-known frequency-down chirp of the QCL. The seed current for the laser generates heat during the pulse which, in turn, makes the frequency decrease throughout the duration of the laser pulse. In order to illustrate this, the frequency chirp of the 8.35 μm laser was studied in detail (Sec. IV B 1.). The consequences of such bandwidth effects are quantitatively discussed and generalized in Sec. IV B 2. Optical feedback due to reflected light from the cavity mirrors does not provide an explanation for the line shift because the QCL is already tuned out of resonance due to the laser chirp when the reflected light arrives at the laser, ~1–3 ns after the initial emission (for the actual distance between cavity and laser). Multimode behavior of the lasers might be another explanation for apparent line broadening or line shifts. However, FTIR spectra of the QCL emission showed no evidence for this hypothesis. Furthermore, the simultaneously recorded reference spectra were not affected in the same manner.

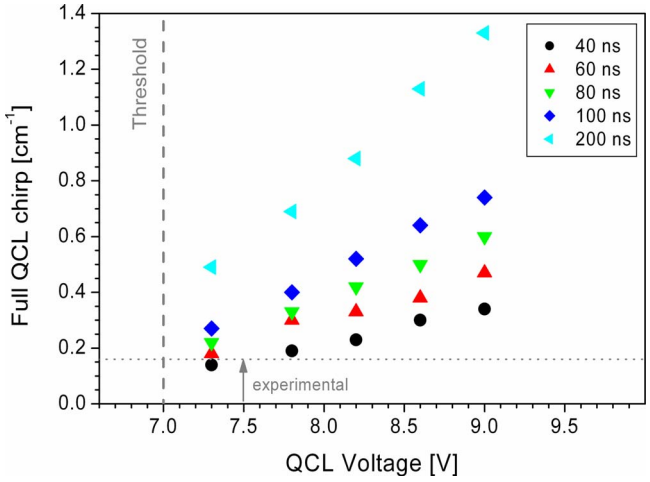

FIG. 9. (Color online) Analysis of the full frequency chirp of the 8.35 μm laser observed for laser pulses of different length and intensity, i.e., for different driving voltages. The voltage threshold of the laser is marked with a dashed vertical line. The chirp expected for the operating conditions of the CRD experiments is indicated by a dotted horizontal line.

1. Determination of the frequency chirp

The frequency chirp of the 8.35 μm laser was evaluated from the direct emission of the QCL (i.e., without the cavity in place and with the current ramp off) modulated with a germanium etalon of 0.048 cm^{-1} free spectral range (FSR). The signal was recorded with a fast TE cooled detector (IPM Freiburg, Vigo element PDI-2TE-10.6). The pulse length was determined from the recorded laser pulse intensities at the noise or zero signal level. Short pulses of less than 40 ns were mainly affected by oscillations originating from the driving current so that the etalon fringes could not be discriminated. For longer pulses all undistorted fringes were analyzed. This resulted in a value for the chirp of the QCL for only a part of the laser pulse, namely, that without current oscillations. For simplicity, it was assumed that the chirp rate of the QCL is constant throughout the laser pulse and hence the full chirp of the laser was extrapolated on the basis of the deduced partial chirp value and the measured total pulse length. Figure 9 shows the full chirp of the QCL for different combinations of operating voltage and pulse length.

In order to increase the usable output signal of the cavity in a CRDS experiment the input can be increased either by modifying the driving voltage or the pulse width. Both factors significantly increase the full chirp of the QCL. It can be seen (Fig. 9) that for operating voltages close to threshold with small pulse widths, e.g., 32 ns, as used here, the chirped QCL pulse should nevertheless cover at least 0.1 cm^{-1} or 3 GHz. In order to verify this for the same QCL operating conditions as in the previous CRDS measurements a 76.2 mm long germanium etalon (0.0163 cm^{-1} FSR) was used. The QCL was swept by a current ramp and each pulse in the train of 160 pulses was recorded. Figure 10 shows an example for one pulse in which a full frequency chirp of about

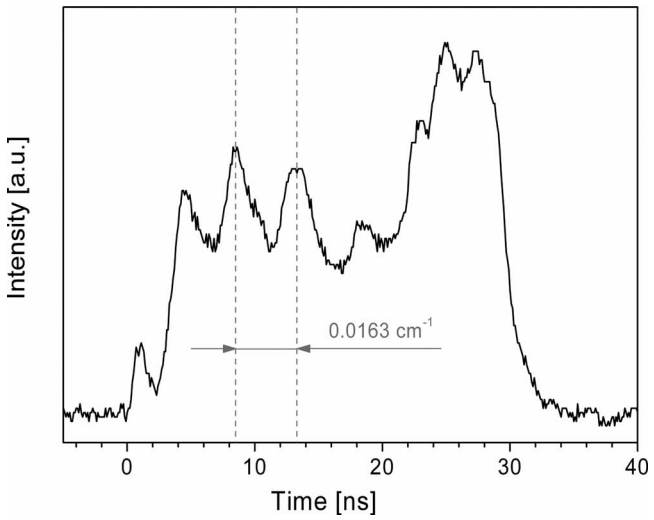

FIG. 10. Example of the QCL chirp for one 32 ns pulse of the 8.35 μm laser at 90% of the applied current ramp, displayed with the aid of a 76.2 mm germanium etalon (0.016 cm^{-1} FSR).

0.16 cm^{-1} (4.8 GHz) was confirmed. The chirp rate of the laser is 0.005 cm^{-1}/ns which accords with the values found for pulsed QCLs by other groups.[48,49,66]

2. Consequences of the chirped pulse

The consequences of such a spectrally extended laser pulse are depicted schematically in Fig. 11. A sample absorption feature of 0.03 cm^{-1} (900 MHz) full width at half maximum (FWHM) is shown as might be observed at intermediate or atmospheric pressures. The upper panel in Fig. 11 is an idealized representation in a theoretical high finesse cavity. Two aspects should be noted. First, the mode structure of the 0.432 m long cavity with a FSR of 0.012 cm^{-1} (360 MHz) was calculated using the expressions given by Zalicki and Zare.[60] Since the excitation of the cavity with 32 ns (or even the 60 ns pulses) neither matches the special case of being twice the round trip time nor being longer than the decay time the idealized picture of an excitation longer than the decay time has been chosen. This would of course only be true for cw illumination of the resonator. The arguments about the effects connected with the chirped QCL pulse are, however, not influenced by this choice. Second, the laser linewidth has been set to 0.0012 cm^{-1} (36 MHz) which is typical for a nonchirped cw QCL with modest power supply ripple.[54] Hence the upper panel of Fig. 11 describes the ideal case for an optical resonator based spectroscopic experiment, where $\Delta\nu_{\text{laser}} < \Delta\nu_{\text{FSR,cav}} < \Delta\nu_{\text{FWHM,line}}$ yielding single exponential decays.

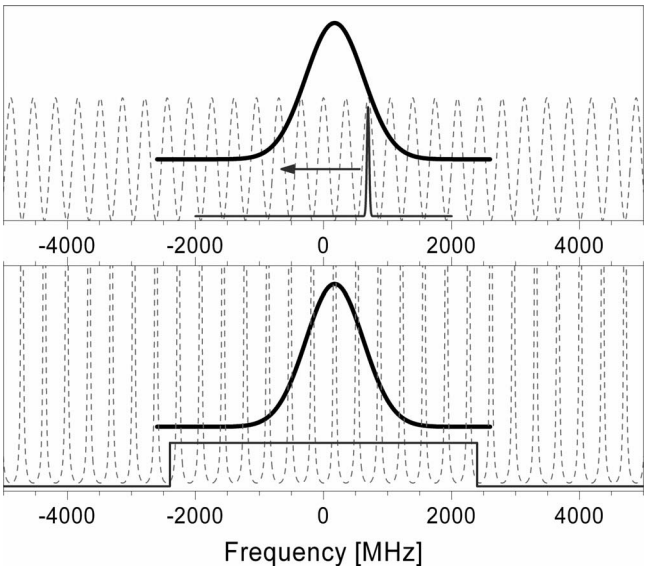

FIG. 11. Simulation of the spectrum of a 43.2 cm long cavity (FSR 360 MHz, dashed) combined with a molecular absorption line (FWHM 900 MHz, solid thick) and the idealized frequency coverage of the QCL emission (solid narrow line) with a laser linewidth of 36 MHz (upper), and for the experimentally observed case with a frequency chirp covering 4.8 GHz (lower).

If now the chirped QCL pulse is taken into account the picture has to be modified. Although this situation has been considered earlier by Silva *et al.*[8] and Sukhorukov *et al.*,[49] the effect is usually underestimated. Silva *et al.* determined an upper limit for the effective laser linewidth of their pulsed QCL, from a fit to NO absorption lines, to be 0.024 cm^{-1}. Since the FSR of their cavity and the absorption features were comparable in width to those presented here (Fig. 11) they concluded that the QCL excites several cavity modes but still fewer than the number encompassed by the absorption feature. The ratio between the absorption linewidth $\Delta\nu_{\text{FWHM,line}}$ and the effective laser linewidth $\Delta\nu_{\text{laser}}$ is the important criterion and strongly depends on the QCL being used. Duxbury *et al.*[66] gave an expression to estimate $\Delta\nu_{\text{laser}}$ for a chirped QCL pulse: $\Delta\nu_{\text{laser}}=(C\ d\nu/dt)^{1/2}$, where $d\nu/dt$ is the chirp rate of the QCL and $C \leq 1$ is a constant. For the 8.35 μm QCL used here $\Delta\nu_{\text{laser}}$ would be 0.013 cm^{-1} (390 MHz) for the limiting case of $C=1$. In the context of Fig. 11 this would lead to the same conclusion as in the case of Silva *et al.* However, the expression for $\Delta\nu_{\text{laser}}$ was derived for a best aperture time Δt. By adjusting the QCL pulse width to facilitate a detectable cavity output this best aperture time is exceeded. Duxbury *et al.* also pointed out that more generally $\Delta t \Delta\nu_{\text{laser}} \geq C$ is valid, i.e., the spectral width of a chirped pulse is determined by the pulse width and/or the Fourier transform limited laser linewidth. Hence, for considerably long QCL pulses, the chirp set by the pulse width is the dominating factor. For the 8.35 μm QCL the full chirp covers 0.16 cm^{-1} (4.8 GHz) which drastically changes the picture, as shown at the bottom panel of Fig. 11. With a single laser pulse almost twice the number of cavity modes are excited than are affected by a representative broad absorption feature at intermediate pressure $\geq$50 mbar.

The consequences are (i) nonexponential decays, (ii) reduced absorptive losses since a part of the injected power is transmitted via undamped cavity modes, and (iii) an apparent line broadening since the absorption feature is present in the decay signal for a much larger number of pulses. All these features are apparent in the results described in Sec. IV A. Laser bandwidth effects of this type were described extensively by Hodges *et al.*[67] for a 3 GHz linewidth dye laser used to probe a 900 MHz (FWHM) absorption feature. They observed five to eight times smaller absorptive losses compared to using a Ti:Al_2O_3 laser source having a bandwidth

smaller than the absorption line. This reduction in sensitivity accords well with the approximately ten times smaller absorption coefficients reported in Sec. IV A

The conclusion from this section is that an infrared source with much smaller effective linewidth or spectral coverage is needed to reach the ideal case of a high finesse cavity experiment suggested by the upper panel in Fig. 11. Since the frequency-down chirp is inherent to pulsed QCLs and no other material combinations are envisaged to reduce the heating of the active core which would slow down the chirp the only solution appears to be the use of cw QCLs. It should be pointed out that the chirped laser pulse is counter productive in two ways that may be synergistic. First, the chirp rate of 150 MHz/ns causes an insufficient cavity buildup because each cavity mode only coincides with the corresponding spectral part of the laser emission for a very short time. This corresponds in fact to a laser pulse at a fixed frequency shorter than the cavity round trip time propagating in the cavity. The throughput is then limited by the reflectivity of the mirrors.[60] For slightly longer interaction with the cavity the intensity gain in the developing cavity modes is still rather limited and so is the output power of the cavity. Second, the full chirp of the QCL excites too many resonator modes as discussed above. In order to achieve a higher cavity output the pulse length or the operating voltage has to be raised which in turn increases the chirp rate and the full chirp respectively, so even more cavity modes are excited during one laser pulse while the interaction time may even be reduced.

C. CEAS using a cw QCL

1. Calibration of the method and test of validity

A room-temperature cw QCL combined with the optical resonator used earlier was applied to perform CEAS experiments. Due to small instabilities in the current source for the QCL the (model) laser linewidth of 0.0012 cm^{-1} suggested in the top panel of Fig. 11 is expected to be a lower limit in practice. From fits to the recorded spectra an upper limit of 0.005 cm^{-1} was deduced taking into account the whole instrumental broadening including data acquisition electronics. This was still sufficient to fall below the absorption linewidth and the cavity mode spacing. The laser is swept by means of a current ramp and probes the absorption feature with the spectral resolution of the cavity FSR.

Spectra of N_2O from different mixtures were recorded, in order to determine the effective reflectivity of the cavity mirrors, and provide a calibration. The measurements were taken under flowing conditions at a constant pressure of 1.2 mbar while the N_2 buffer gas and N_2O flow was varied for the different N_2O calibrations. Figure 12 shows the result of the spectral scans, obtained with a LN cooled detector, and averaged over 20 s. Lower intensity N_2O lines, just exceeding the noise level $\sim 2\times 10^{-3}$ in transmission, can be seen between the three dominant N_2O features in the spectrum at 100 ppm. The line positions and line strengths from the HITRAN database are given in Table I.[61] The relative absorption of the two lines with a line strength of nearly 10^{-20} cm/molecule was 17% in the 100 ppm N_2O sample.

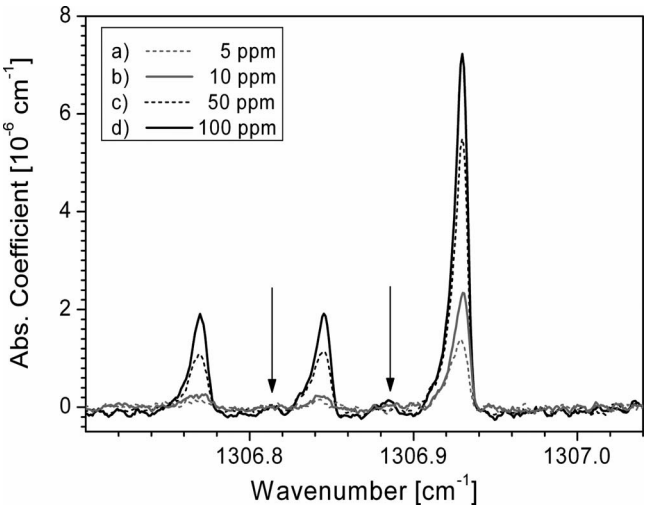

FIG. 12. CEAS scans for different N_2O calibration mixtures (N_2O diluted in N_2) at a constant total pressure of 1.2 mbar: (a) 5 ppm, (b) 10 ppm, (c) 50 ppm, and (d) 100 ppm. The acquisition time was 20 s. The weak absorption features indicated by arrows appear above noise level only in the spectrum at 100 ppm.

Even for such comparatively small absorptions a correction for nonlinearity is recommended (see below). A fit of the transmission spectra resulted in an effective reflectivity of $R=99.96\%$ for the cavity mirrors or an effective path length of 1080 m. Since in this approach the excitation of high order transverse modes may occur which could have different diffraction losses, this value of R should be regarded as an effective one.[50] No evidence was found that optical feedback from the cavity to the QCL caused line shifts or perturbed lines. The three strong N_2O lines visible in Fig. 12 have been analyzed further using Eq. (13) which provides a means of checking the validity of the weak absorber assumption. For this purpose $\ln(I_0/I)\approx GA$ at the maximum was plotted against the concentration of N_2O in the cavity (Fig. 13). Due to its order of magnitude higher line strength compared to the other lines, the data for the line at 1306.93 cm^{-1} is nonlinear even for number densities in the 10^{11} molecules/cm^3 range. For the two smaller lines, which have approximately the same line strength, the linear assumption is valid at least up to $\sim 1\times 10^{12}$ molecules/cm^3. Generally, it can be concluded that the linear approximation is valid for $GA\leq 0.15$ while for absorption features bigger than 15% a correction is necessary.

Finally the CEAS system was validated with measurements on constituents of laboratory air, namely, CH_4, N_2O,

TABLE I. N_2O line strengths and line positions observed in the calibration experiments. The data indicated with ($*$) were used for further analysis.

Line position ν (cm^{-1})	Line strength S (cm/molecule)
1306.771 21*	9.72×10^{-21}
1306.815 72	6.13×10^{-22}
1306.846 08*	9.72×10^{-21}
1306.887 14	5.36×10^{-22}
1306.887 39	5.36×10^{-22}
1306.929 12*	1.04×10^{-19}

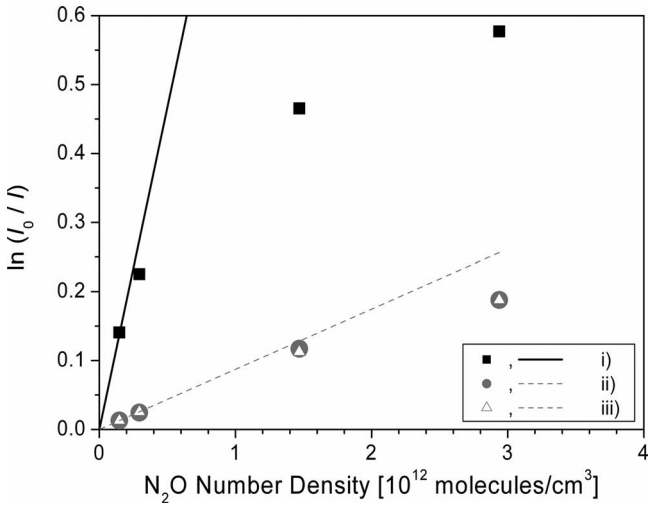

FIG. 13. Calibration data for the maxima of the three absorption lines and the four mixing ratios of N_2O mentioned in Fig. 12: (i) 1306.929 cm^{-1}, (ii) 1306.846 cm^{-1}, and (iii) 1306.771 cm^{-1}.

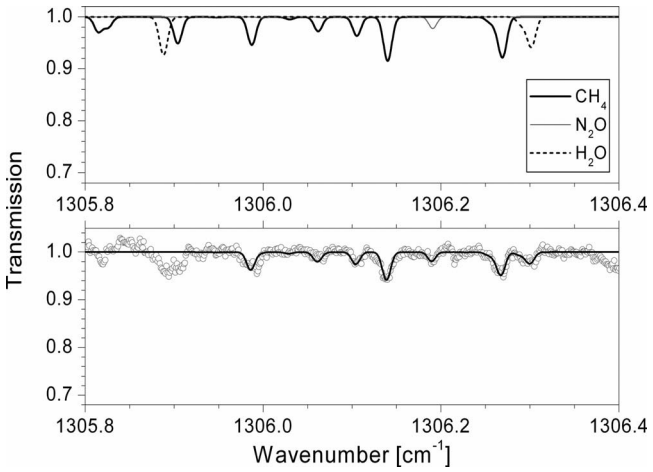

FIG. 14. Calculated spectrum (upper) for air containing CH_4, N_2O, and H_2O. Experimental conditions: $p=2.2$ mbar, $L_{eff}=1080$ m, and 0.005 cm^{-1} instrumental broadening. The corresponding CEAS spectrum (lower) was observed with a TE cooled detector (open circles) and fitted (solid line) to determine the actual concentrations.

and H_2O, which could be detected within one spectral scan. The spectrum expected to arise for the average mixing ratios of the three molecules was calculated and is plotted in the upper panel of Fig. 14. Some noninterfering absorption features were selected for analysis and these are summarized in Table II. Since the water lines are of low line strengths the large amounts of H_2O in air compared to the other trace gases could be examined. The single water line in the spectrum consists of two unresolved lines with a spacing of 0.004 cm^{-1}, so that an effective value for S (for simplicity the sum) is used. A third line shifted by ~0.010 cm^{-1} with a line strength of only 20% of the effective S of the unresolved neighbor appears as a shoulder to the left of the main line(s). This transition was deconvoluted from the main lines and was not used for the quantitative analysis. The transmission spectrum recorded with a TE cooled detector is shown in the lower panel of Fig. 14. The measurements were performed under flowing and with low pressure conditions at 2.2 mbar in order to increase line selectivity. The spectrum was averaged for 20 s. Qualitatively it agrees very well with the simulation. The line positions were fitted to a transmission profile which is also plotted in Fig. 14. This fit was then used to calculate the absorption coefficient using Eq. (12). Integrating over the absorption line of interest revealed the number density and mixing ratio. The results of this quantitative analysis are given in Table II: 1.7 ppm of CH_4, 350 ppb N_2O, and more than 1% of water. A comparison with literature values for the abundance of these molecules in air (1.75 ppm for CH_4, 320 ppb for N_2O, and 0.1%–4% for H_2O) yields fair agreement.[3,68]

2. System performance

In order to be able to evaluate the sensitivity of the TE cooled system the measurements on laboratory air were repeated with a LN cooled detector and the results were very similar. Furthermore, the relative measurement error after 20 s was almost the same ($\Delta I/I_0$ of 0.3% for the TE detector, 0.2% for the LN cooled detector). The corresponding NEA is then 1.8×10^{-7} cm^{-1} $Hz^{-1/2}$ for the TE detector if the calibration error in R is included as given by Eq. (19). The system was aligned on-axis with respect to the laser beam which produces cavity mode noise inherent to ICOS/CEAS setups.[55] In order to achieve an accurate SNR, a measurement interval of at least 5 s is necessary to smooth out the residual mode structure on the base line. It is possible to estimate the minimum detectable number density (MDND) n_{min} for each molecule by means of the absorption coefficient k_{min}. The approximation $n_{min}S=k_{min}\Delta\nu_{line}/2(\pi/\ln 2)^{1/2}$ was used,[69] assuming that k_{min} corresponds to the maximum of the smallest absorption feature that can be distinguished from the noise. This approximation is only valid at low pressures where the FWHM absorption linewidth $\Delta\nu_{line}$ is dominated by Doppler broadening. The MDNDs of the different

TABLE II. Species detected in ambient laboratory air at 2.2 mbar (n-number density).

Molecule	ν (cm^{-1})	Line strength S (cm/molecule)	Mixing ratio	n (molecules/cm^3)	MDND (n_{min}) (molecules/cm^3)
CH_4	1305.987	4.78×10^{-20}	1.72 ppm	9.2×10^{10}	2.5×10^{9}
CH_4	1306.062	2.41×10^{-20}	1.82 ppm	9.8×10^{10}	4.9×10^{9}
CH_4	1306.105	3.19×10^{-20}	1.68 ppm	9.0×10^{10}	3.7×10^{9}
CH_4	1306.140	7.60×10^{-20}	1.66 ppm	8.9×10^{10}	1.6×10^{9}
N_2O	1306.191	1.12×10^{-19}	346 ppb	1.9×10^{10}	6.4×10^{8}
H_2O	1306.29	6.08×10^{-24} [a]	1.1%	5.8×10^{14}	1.8×10^{13}

[a]Effective line strength from two unresolved lines.

TABLE III. Intercomparison of high sensitivity QCL based spectrometers employing optical cavities, long path cells, or PAS.

Ref.	Method	λ (μm)	QCL	Operating temperature	Detector cooling	L_{eff} (m)	NEA[a] (cm^{-1} $Hz^{-1/2}$)	Gas	MDND[b] (molecules/cm^3)	Recording time (s)
48 and 62	CRDS	10.3	Pulsed	Near ambient	Cryogenic	240	5×10^{-6}	NH_3	1.2×10^{12}	20
53 and 70	CRDS	5.2	cw	Cryogenic	Cryogenic	1050[a]	1×10^{-7}	NO	1.4×10^{9}	8
46 and 71	CRDS	8.5	cw	Cryogenic	Cryogenic	280[a]	4×10^{-9} [c]	NH_3	6.7×10^{9}	1
50 and 72	CEAS	5.2	cw	Cryogenic	TE	670	3×10^{-6}	NO	1.6×10^{10}	200
58 and 73	ICOS (off-axis)	3.5	cw[d]	Cryogenic	Cryogenic	83[a]	5×10^{-7}	H_2CO	1.6×10^{11}	3
52 and 74	ICOS[e]	5.2	cw	Cryogenic	Cryogenic	75	2×10^{-7}	NO	3.3×10^{10}	15
This work	CEAS	7.7	cw	Near ambient	TE	1080	2×10^{-7}	CH_4	1.6×10^{9}	20
								N_2O	6.4×10^{8}	20
54 and 75	ICOS[e]	5.5	cw	Near ambient	Cryogenic	700	1×10^{-7}	NO	2.1×10^{10}	1
8 and 63	ICOS	5.2	Pulsed	Near ambient	Cryogenic	1500	6×10^{-8}	NO	$\sim2\times10^{9}$	4
55 and 76	ICOS	5.5	cw	Near ambient	Cryogenic	500	4×10^{-8}	NO	1.2×10^{10}	4
51 and 77	ICOS (off-axis)	7.9	cw	Cryogenic	Cryogenic	5560[a]	2×10^{-9} [c]	CH_4	2.9×10^{9}	10
47	CEAS (locked)	8.7	cw				8×10^{-10} [c]	N_2O		
47	NICE-OHMS	8.7	cw				1×10^{-10} [c]	N_2O		
44 and 78	QCLAS[f]	4.3	Pulsed	Near ambient	TE	56	1×10^{-7}	CO_2	5.3×10^{8}	240
50 and 64	QCLAS[f]	5.2	cw	Cryogenic	TE	100	3×10^{-8}	NO	4.2×10^{9}	200
43 and 79	QCLAS[f]	7.9	Quasi-cw	Cryogenic	Cryogenic	100	2×10^{-8}	CH_4	$\sim2\times10^{9}$	30
								N_2O	$\sim7\times10^{8}$	30
1 and 80	QCLAS[f]	7.9	Pulsed	Near ambient	TE	56	2×10^{-8}	CH_4	1.1×10^{9}	200
								N_2O	5.9×10^{9}	1
1 and 81	QCLAS[f]	4.5	Pulsed	Near ambient	TE	56	7×10^{-9}	N_2O	6.9×10^{7}	100
38 and 65	QCLAS[f]	5.3	cw	Near ambient	TE	210	3×10^{-10}	NO	2.0×10^{7}	30
39 and 82	QCLAS[f]	5.3	Pulsed	Near ambient	Cryogenic	210	5×10^{-10} [c]	NO	1.9×10^{8}	1
					TE	210	1×10^{-9} [c]	NO	4.1×10^{8}	1
41 and 83	PAS	7.9	cw	Cryogenic/ambient	…	…	$\sim9\times10^{-7}$	CH_4	8.4×10^{11}	$\sim$150
								N_2O	3.5×10^{11}	$\sim$150
42 and 84	QEPAS[g]	4.6	cw	Cryogenic	…	…	8×10^{-7}	N_2O	6.5×10^{9}	[h]
40 and 85	QEPAS[g]	8.4	External cavity	Near ambient	…	…	4×10^{-7}	C_2HF_5	2.5×10^{9}	100

[a]Value estimated by the authors from the cited data.
[b]Calculated from $n=p/k_BT$ multiplied by the best reported concentration or mixing ratio; normally $T=296$ K.
[c]Original value given in the reference.
[d]ICL.
[e]In combination with wavelength modulation the sensitivity was approximately times better.
[f]QCL absorption spectroscopy.
[g]Quartz enhanced PAS.
[h]3 s time constant for a single spectral position.

molecules analyzed are listed in Table II. For N_2O a detection limit of 6.4×10^{8} molecules/cm^3 is obtained, which transferred to CH_4 corresponds to 1.6×10^{9} molecules/cm^3 for the strongest line in CH_4. If this is converted into a mixing ratio at 2.2 mbar, where the TE spectrum was acquired, the limits of detection for N_2O and CH_4 are 12 ppb (parts per 10^9) and 46 ppb, respectively, for a 20 s measurement interval. Using the LN cooled detector these limits would be reduced by a factor of 2/3 due to a reduced $\Delta I/I_0$. Clearly for measurements at intermediate or atmospheric pressures sub-ppb levels can be measured although the lines would be broader and might be unresolved.

The sensitivity achieved with the CEAS system is comparable to other QCL based high finesse cavity spectrometers reported in literature. The main parameters of those and the CEAS system studied here are collected in Table III. To facilitate intercomparisons the specifications of the different systems were converted into the NEA and the MDND for the different molecules. The MDND typically represents the best reported value, sometimes achieved with extended averaging, e.g., determined from Allan variance plots. In some cases the scaling of the NEA with $f^{-1/2}$ according to Eq. (19) does not hold. Therefore the given NEA values should be considered as estimates for short term measurements ($\sim$1 s) and may not be directly converted in all cases to the MDND.

The sensitivity of 1.8×10^{-7} cm^{-1} $Hz^{-1/2}$ presently achieved with the entirely TE cooled CEAS system demonstrates a better performance than CRDS setups with pulsed QCLs, as discussed in Sec. IV A 3 and is comparable to several other CEAS or ICOS studies exhibiting a NEA down to 4×10^{-8} cm^{-1} $Hz^{-1/2}$.[50,52,54,55,58] It is still almost a factor of $\sim$50 less sensitive than CRDS employing a cw QCL as demonstrated by Paldus *et al.*,[46] which may be explained by the commonly omitted cavity mode noise in CRDS. For CEAS or ICOS the minimum detectable absorption is typically lim-

ited to 10^{-2}–10^{-3} due to incomplete averaging over the cavity resonances. In combination with wavelength modulation techniques this can be improved by a factor of ~5 (Refs. 52 and 54) at the expense of a more complex experimental layout. Another approach to increase the SNR in the spectra is an off-axis alignment requiring mirrors of bigger diameter. A sensitivity of 2×10^{-9} cm^{-1} $Hz^{-1/2}$ was reported with a cavity base length L less than twice as long as presented here.[51] The MDND achieved for CH_4 at 7.9 μm with this method was 2.9×10^{9} molecules/cm^3 compared to 1.6×10^{9} molecules/cm^3 in the present study due an advantageous spectral position and a lower sampling pressure in our experiment. Not surprisingly the sensitivity of the system described here cannot compete with the values obtained with sophisticated locked CEAS setups (8×10^{-10} cm^{-1} $Hz^{-1/2}$) or even with NICE-OHMS (9.7×10^{-11} cm^{-1} $Hz^{-1/2}$).[47] Apart from the limitations in the SNR inherent to the CEAS approach, the currently achieved detection limits could be further improved using the nearly ten times stronger absorption band at 4.5 μm for N_2O or the 3 μm region for CH_4. The latter spectral range requires ICLs that have recently become available.

QCL spectrometers employing conventional long path cells which are today increasingly based on TE cooled lasers and detectors accomplish sensitivities well below 1×10^{-7} cm^{-1} $Hz^{-1/2}$ (Table III) even down to 3×10^{-10} cm^{-1} $Hz^{-1/2}$ (Refs. 38 and 65) and hence are still superior to CEAS or ICOS setups. The main reason is the residual mode noise which is absent in the spectra for those spectrometers. However, the aim has been to achieve maintenance free operation with a small sample volume, presently around 0.3 l, and with an optical geometry reduced in its complexity which would make the system field deployable. The volume of the multiple pass cells listed in Table III, covering effective path lengths up to 210 m, typically ranges from 0.5 to 5 l which may increase the dimensions of the system and the necessary pumping time. More recently, photoacoustic spectroscopy (PAS) has been reported using LN and TE cooled cw QCL (Ref. 41) or external cavity lasers.[40] Detection limits in the order of ~10^{-7} cm^{-1} $Hz^{-1/2}$, but still inferior to methods applying optical cavities, were obtained (Table III). Moreover, the acquisition time for photoacoustic spectra is rather long (approximately minutes), which does not enable real-time measurements to be performed.

V. CONCLUSIONS

TE cooled QCLs have been combined with high finesse optical resonators in order to profit from their enlarged path lengths at reasonably small sample volumes in combination with the high absorption cross section in the infrared molecular fingerprint region. Two different approaches have been investigated. First, pulsed QCLs at 7.42 and 8.35 μm were used to perform CRDS and ICOS experiments. The spectra measured at pressures between 100 and 300 mbar were normally characterized by a broadening of the absorption lines and reduced absorption in comparison with theoretical expectations, which makes an absolute calibration necessary. The resulting decrease in sensitivity, i.e., to ~5×10^{-7} cm^{-1} $Hz^{-1/2}$, means that long path cell configurations of similar sample volumes have superior sensitivity to either CRDS or ICOS. It transpires that the frequency-down chirp inherent to pulsed QCLs sets the fundamental limit. Due to the chirp the effective linewidth of the QCL is much broader than the narrow molecular absorption features and the rather fast chirp rate does not allow for an efficient buildup of the laser field in the cavity. CRDS using pulsed QCLs therefore has only a limited number of useful applications, e.g., for the determination of the reflectivity of the cavity mirrors in preliminary experiments or for the detection of complex and broad molecular absorptions at higher pressures. Second, a cw QCL at 7.66 μm has been combined with an unstabilized and unlocked cavity. With this straightforward arrangement, comprising only a TE cooled detector, an effective path length of 1080 m has been achieved. The main limit to sensitivity, of 2×10^{-7} cm^{-1} $Hz^{-1/2}$, was the cavity mode noise which may be reduced by off-axis alignment. Such mode noise is absent in conventional long path cell spectrometers which hence exhibit a higher sensitivity. With a 20 s measurement interval detection limits for N_2O and CH_4 of 6×10^{8} and 2×10^{9} molecules/cm^3, respectively, could be achieved at 2.2 mbar indicating that sub-ppb levels could easily be measured at higher pressures. Furthermore, the small sample volume of 0.3 l used here, and consequently the reduced pumping requirement, is an advantage over long path cells with much larger volumes than 0.5 l. The detection limits achieved here are relevant both for the detection of radicals in plasma chemistry and for trace gas measurements with field-deployable systems. Additionally, trace gas measurements may also be carried out without preconcentration procedures. Radicals with small abundances in the gas phase might now be detectable via QCL based spectroscopy. The choice of an appropriate method depends on whether the important criterion is ultimate sensitivity or a more compact system. In the former case a multipass cell spectrometer would be preferable because of its better signal–to-noise characteristics but this configuration would exclude the detection of processes on short time scales or certain types of *in situ* measurements. Sophisticated locked cavity schemes might overcome such restrictions at the expense of complex spectrometer geometries. To achieve a compact system a small volume cavity based spectrometer employing cw QCLs would be more appropriate. This configuration would also be of special interest for applications where the pressure cannot arbitrarily be chosen in order to adapt the absorption linewidth to the laser linewidth, e.g., in low pressure plasmas. Moreover, for these applications *in situ* measurements are essential because multipass cell sampling *ex situ* is not an option.

ACKNOWLEDGMENTS

The authors thank P. Vankan and R. Zijlmans for supplementary information and useful discussions. S. Glitsch, D. Gött, U. Macherius, S. Saß, and F. Weichbrodt provided valuable technical assistance for which we are grateful. The authors are also indebted to Alpes Lasers for supporting the work. In addition, the project was supported by the German

Research Foundation (DFG) within the framework of the Collaborative Research Centre Transregio 24 "Fundamentals of Complex Plasmas."

[1]D. D. Nelson, B. McManus, S. Urbanski, S. Herndon, and M. S. Zahniser, Spectrochim. Acta, Part A **60**, 3325 (2004).
[2]J. H. Steinfeld and S. N. Pandis, *Atmospheric Chemistry and Physics: From Air Pollution to Climate Change* (Wiley, New York, 1998).
[3]S. S. Brown, Chem. Rev. (Washington, D.C.) **103**, 5219 (2003).
[4]J. Röpcke, G. Lombardi, A. Rousseau, and P. B. Davies, Plasma Sources Sci. Technol. **15**, S148 (2006).
[5]G. D. Stancu, N. Lang, J. Röpcke, M. Reinicke, A. Steinbach, and S. Wege, Chem. Vap. Deposition **13**, 351 (2007).
[6]H. Gupta and L. S. Fan, Ind. Eng. Chem. Res. **42**, 2536 (2003).
[7]C. Bauer, P. Geiser, J. Burgmeier, G. Holl, and W. Schade, Appl. Phys. B: Lasers Opt. **85**, 251 (2006).
[8]M. L. Silva, D. M. Sonnenfroh, D. I. Rosen, M. G. Allen, and A. O'Keefe, Appl. Phys. B: Lasers Opt. **81**, 705 (2005).
[9]M. W. Todd, R. A. Provencal, T. G. Owano, B. A. Paldus, A. Kachanov, K. L. Vodopyanov, M. Hunter, S. L. Coy, J. I. Steinfeld, and J. T. Arnold, Appl. Phys. B: Lasers Opt. **75**, 367 (2002).
[10]M. R. McCurdy, Y. Bakhirkin, G. Wysocki, R. Lewicki, and F. K. Tittel, J. Breath Res. **1**, 014001 (2007).
[11]A. O'Keefe and D. A. G. Deacon, Rev. Sci. Instrum. **59**, 2544 (1988).
[12]R. Engeln, G. Berden, R. Peeters, and G. Meijer, Rev. Sci. Instrum. **69**, 3763 (1998).
[13]A. O'Keefe, J. J. Scherer, and J. B. Paul, Chem. Phys. Lett. **307**, 343 (1999).
[14]A. O'Keefe, Chem. Phys. Lett. **293**, 331 (1998).
[15]M. Mürtz, B. Freech, and W. Urban, Appl. Phys. B: Lasers Opt. **68**, 243 (1999).
[16]J. Ye, L. S. Ma, and J. L. Hall, J. Opt. Soc. Am. B **15**, 6 (1998).
[17]D. Romanini, A. A. Kachanov, and F. Stoeckel, Chem. Phys. Lett. **270**, 538 (1997).
[18]G. Berden, R. Peeters, and G. Meijer, Chem. Phys. Lett. **307**, 131 (1999).
[19]*Cavity Ring-Down Spectroscopy: An Ultratrace Absorption Measurement Technique*, edited by K. W. Busch and M. A. Busch (American Chemical Society, Washington, DC, 1999).
[20]J. J. Scherer, D. Voelkel, D. J. Rakestraw, J. B. Paul, C. P. Collier, R. J. Saykally, and A. O'Keefe, Chem. Phys. Lett. **245**, 273 (1995).
[21]J. J. Scherer, K. W. Aniolek, N. P. Cernansky, and D. J. Rakestraw, J. Chem. Phys. **107**, 6196 (1997).
[22]S. Wu, P. Dupré, and T. A. Miller, Phys. Chem. Chem. Phys. **8**, 1682 (2006).
[23]F. Ito, J. Chem. Phys. **124**, 054309 (2006).
[24]J. B. Paul and R. J. Saykally, Anal. Chem. **69**, 287 (1997).
[25]J. B. Paul, R. A. Provencal, C. Chapo, K. Roth, R. Casaes, and R. J. Saykally, J. Phys. Chem. A **103**, 2972 (1999).
[26]J. B. Paul, R. A. Provencal, C. Chapo, A. Petterson, and R. J. Saykally, J. Chem. Phys. **109**, 10201 (1998).
[27]R. Peeters, G. Berden, A. Olafsson, L. J. J. Laarhoven, and G. Meijer, Chem. Phys. Lett. **337**, 231 (2001).
[28]D. Kleine, H. Dahnke, W. Urban, P. Hering, and M. Mürtz, Opt. Lett. **25**, 1606 (2000).
[29]D. Halmer, G. von Basum, P. Hering, and M. Mürtz, Opt. Lett. **30**, 2314 (2005).
[30]M. M. Hemerik and G. M. W. Kroesen, presented at the Frontiers in Low Temperature Plasma Diagnostics IV, Rolduc, The Netherlands, 25–29 March 2001 (unpublished).
[31]M. Hemerik, Ph.D. thesis, Eindhoven University of Technology, 2001.
[32]J. Remy, M. M. Hemerik, G. M. W. Kroesen, and W. W. Stoffels, IEEE Trans. Plasma Sci. **32**, 709 (2004).
[33]J. Faist, F. Capasso, D. L. Sivco, C. Sirtori, A. L. Hutchinson, and A. Cho, Science **264**, 553 (1994).
[34]R. Q. Yang, C. J. Hill, B. H. Yang, C. M. Wong, R. E. Muller, and P. M. Echternach, Appl. Phys. Lett. **84**, 3699 (2004).
[35]R. Q. Yang, C. J. Hill, and B. H. Yang, Appl. Phys. Lett. **87**, 151109 (2005).
[36]M. Beck, D. Hofstetter, T. Aellen, J. Faist, U. Oesterle, M. Ilegems, E. Gini, and H. Melchior, Science **295**, 301 (2002).
[37]C. Roller, A. A. Kosterev, F. K. Tittel, K. Uehara, C. Gmachl, and D. L. Sivco, Opt. Lett. **28**, 2052 (2003).
[38]D. D. Nelson, J. B. McManus, S. C. Herndon, J. H. Shorter, M. S. Zahniser, S. Blaser, L. Hvozdara, A. Muller, M. Giovannini, and J. Faist, Opt. Lett. **31**, 2012 (2006).
[39]D. D. Nelson, J. H. Shorter, J. B. McManus, and M. S. Zahniser, Appl. Phys. B: Lasers Opt. **75**, 343 (2002).
[40]R. Lewicki, G. Wysocki, A. A. Kosterev, and F. K. Tittel, Opt. Express **15**, 7357 (2007).
[41]A. Grossel, V. Zeninari, B. Parvitte, L. Joly, and D. Courtois, Appl. Phys. B: Lasers Opt. **88**, 483 (2007).
[42]A. A. Kosterev, Y. A. Bakhirkin, and F. K. Tittel, Appl. Phys. B: Lasers Opt. **80**, 133 (2005).
[43]A. A. Kosterev, R. F. Curl, F. K. Tittel, C. Gmachl, F. Capasso, D. L. Sivco, J. N. Baillargeon, A. L. Hutchinson, and A. Y. Cho, Appl. Opt. **39**, 4425 (2000).
[44]B. Tuzson, M. J. Zeeman, M. S. Zahniser, and L. Emmenegger, Infrared Phys. Technol. **51**, 198 (2008).
[45]J. B. McManus, P. L. Kebabian, and M. S. Zahniser, Appl. Opt. **34**, 3336 (1995).
[46]B. A. Paldus, C. C. Harb, T. G. Spence, R. N. Zare, C. Gmachl, F. Capasso, D. L. Sivco, J. N. Baillargeon, A. L. Hutchinson, and A. Y. Cho, Opt. Lett. **25**, 666 (2000).
[47]M. S. Taubman, T. L. Myers, B. D. Cannon, and R. M. Williams, Spectrochim. Acta, Part A **60**, 3457 (2004).
[48]J. Manne, O. Sukhorukov, W. Jäger, and J. Tulip, Appl. Opt. **45**, 9230 (2006).
[49]O. Sukhorukov, A. Lytkine, J. Manne, J. Tulip, and W. Jäger, Proc. SPIE **6127**, 61270A (2006).
[50]L. Menzel, A. A. Kosterev, R. F. Curl, R. F. Tittel, C. Gmachl, F. Capasso, D. L. Sivco, J. N. Baillargon, A. L. Hutchinson, A. Y. Cho, and W. Urban, Appl. Phys. B: Lasers Opt. **72**, 859 (2001).
[51]J. B. Paul, J. J. Scherer, A. O'Keefe, L. Lapson, J. G. Anderson, C. Gmachl, F. Capasso, and A. Y. Cho, Proc. SPIE **4577**, 1 (2002).
[52]Y. A. Bakhirkin, A. A. Kosterev, C. Roller, R. F. Curl, and F. K. Tittel, Appl. Opt. **43**, 2257 (2004).
[53]A. A. Kosterev, A. L. Malinovsky, F. K. Tittel, C. Gmachl, F. Capasso, D. L. Sivco, J. N. Baillargeon, A. L. Hutchinson, and A. Y. Cho, Appl. Opt. **40**, 5522 (2001).
[54]Y. A. Bakhirkin, A. A. Kosterev, R. F. Curl, F. K. Tittel, L. Hvodzdara, M. Giovannini, and J. Faist, Appl. Phys. B: Lasers Opt. **82**, 149 (2006).
[55]M. R. McCurdy, Y. A. Bakhirkin, and F. K. Tittel, Appl. Phys. B: Lasers Opt. **85**, 445 (2006).
[56]F. K. Tittel, Y. Bakhirkin, A. A. Kosterev, and G. Wysocki, Rev. Laser Eng. **34**, 275 (2006).
[57]A. A. Kosterev and F. K. Tittel, IEEE J. Quantum Electron. **38**, 582 (2002).
[58]J. H. Miller, Y. A. Bakhirkin, T. Ajtai, F. K. Tittel, C. J. Hill, and R. Q. Yang, Appl. Phys. B: Lasers Opt. **85**, 391 (2006).
[59]M. Mazurenka, A. J. Orr-Ewing, R. Peverall, and G. A. D. Ritchie, Annu. Rep. Prog. Chem., Sect. C: Phys. Chem. **101**, 100 (2005).
[60]P. Zalicki and R. N. Zare, J. Chem. Phys. **102**, 2708 (1995).
[61]L. S. Rothman, D. Jacquemart, A. Barbe, D. C. Benner, M. Birk, L. R. Brown, M. R. Carleer, C. Chackerian, Jr., K. Chance, L. H. Coudert, V. Dana, V. M. Devi, J.-M. Flaud, R. R. Gamache, A. Goldman, J.-M. Hartmann, K. W. Jucks, A. G. Maki, J.-Y. Mandin, S. T. Massie, J. Orphal, A. Perrin, C. P. Rinsland, M. A. H. Smith, J. Tennyson, R. N. Tolchenov, R. A. Toth, J. Vander Auwera, P. Varanasi, and G. Wagner, J. Quant. Spectrosc. Radiat. Transf. **96**, 139 (2005).
[62]The MDND was calculated with 50 ppb at atmospheric pressure. The NEA was estimated via the minimum round trip loss for 16 ppb standard deviation (Fig. 7 in Ref. 48) and converted into k_{min}. Equation (19) for 20 s averaging (without $\sqrt{2}$) yields the NEA.
[63]Figure 8 in Ref. 8 implies a minimum detectable absorption of 3×10^{-3} for 1500 m in 4 s. The NEA follows from Eqs. (18) and (19) and the MDND from 0.7 ppb at 100 Torr or 0.8 ppb at 70 Torr. Those minimum concentrations are given as rms noise from approximately ten different 4 s scans and are therefore smaller than a minimum absorption of 3×10^{-3} would suggest.
[64]Figure 3 in Ref. 50 implies an absorption of 0.0005 for 13 ppb NO (50 Torr) for a SNR=5, i.e., the minimum detectable absorption is $\sim10^{-4}$. For $N=100$ scans the SNR was improved by $N^{1/2}$ while for 10 000 averages an additional factor 2.5 is achieved, i.e. a factor 25 in total compared to a single scan. The NEA follows from Eqs. (18) and (19) (without $\sqrt{2}$ because $L_{eff}=100$ m was not calibrated).
[65]The Allan variance minimum of 0.03 ppb after 30 s corresponds to 3×10^{-6} absorbance noise and $k_{min}=1.5\times10^{-10}$ cm^{-1}, respectively (Ref.

38). Since the short term noise (1 s) is 0.06 ppb the corresponding values were also scaled by a factor 2, i.e. the NEA is $\sim 3\times10^{-10}$ cm^{-1} $Hz^{-1/2}$. The MDND follows from 0.03 ppb at 20 Torr.

[66]G. Duxbury, N. Langford, M. T. McCulloch, and S. Wright, Chem. Soc. Rev. **34**, 921 (2005).

[67]J. T. Hodges, J. P. Looney, and R. D. van Zee, Appl. Opt. **35**, 4112 (1996).

[68]E. Uherek and R. Sander, ESPERE Climate Encyclopaedia, 2006 (http://www.espere.net/).

[69]Combining Eqs. (1) and (2) without integration yields $L_{\mathrm{eff}}^{-1}\ \ln(I_0/I)=k=nSf(\nu-\nu_0)$, where f describes the line profile. In the case of low pressures (<5 mbar) f can be approximated by a Doppler profile and k or f can be analytically expressed at ν_0, i.e. $L_{\mathrm{eff}}^{-1}\ \ln[I_0(\nu_0)/I(\nu_0)]=k(\nu_0)=nS\times2(\ln 2/\pi)^{1/2}/\Delta\nu_{\mathrm{line}}$, where $\Delta\nu_{\mathrm{line}}$ is the FWHM and thus $nS\sim\ln(I_0/I)$ at the maximum.

[70]L_{eff} was calculated from $\tau_0=3.5$ μs. After 8 s the relative error of τ was 4.7×10^{-3}; Eqs. (17) and (19) yield the NEA (without $\sqrt{2}$ because R was not calibrated). The MDND follows from the detection limit of 0.7 ppb at 60 Torr (Ref. 53).

[71]After 600 scans at 600 Hz the standard deviation was 10^{-4}. The NEA follows from Eqs. (18) and (19) and the MDND from 0.25 ppb detection limit at STP (Ref. 46). L_{eff} was estimated from $\tau_0=0.93$ μs.

[72]The MDND was calculated with 16 ppb at 30 Torr (Ref. 50). A minimum detectable absorption of 0.01 with $L_{\mathrm{eff}}=670$ m in 200 s yields the NEA with Eqs. (18) and (19).

[73]L_{eff} was calculated from $R_{\mathrm{eff}}=99.4\%$ and 50 cm base length. The MDND follows from 100 ppb at 50 Torr whereas the NEA was calculated with 0.15% standard deviation in absorption for 3.3 s averaging and $L_{\mathrm{eff}}=83.3$ m (Ref. 58).

[74]Figure 10 in Ref. 52 implies a minimum detectable absorption of 3×10^{-4} for 75 m in 15 s. The NEA follows from Eqs. (18) and (19) and the MDND from 10 ppb at 100 Torr.

[75]Figure 4 in Ref. 54 implies a minimum detectable absorption of 6×10^{-3} for 700 m in 1 s. The NEA follows from Eqs. (18) and (19) and the MDND from 3.2 ppb at 200 Torr.

[76]Figure 5 in Ref. 55 implies a minimum detectable absorption of 6×10^{-4} for 500 m in 4 s. The NEA follows from Eqs. (18) and (19) and the MDND from 3.6 ppb at 100 Torr.

[77]With the given gain factor 6760 R_{eff} is estimated to be 99.9852%. Consequently L_{eff} is 5560 m for a base length of 82.3 cm. The MDND follows from the 3 ppb detection limit at 30 Torr (Ref. 51).

[78]The MDND was calculated from the Allan variance minimum of 0.12 ppm at 14 Torr after 240 s corresponding to a peak absorbance precision of 6×10^{-5}. This value was scaled with ~10 since it does not scale with the square root of averages (Ref. 44) to determine the short term deviation (1 s) yielding 1.1 ppm. The NEA follows from Eqs. (18) and (19) for 56 m path length.

[79]The MDND was calculated for the smallest pressure given in Ref. 43 (20 Torr) and 2.5 ppb CH_4 and 1.0 ppb N_2O, respectively. The NEA follows from Eqs. (18) and (19) (without $\sqrt{2}$) for 3.5×10^{-5} minimum peak absorbance, 30 s averaging, and 100 m path length.

[80]The NEA follows from Eqs. (18) and (19) for 1.4×10^{-4} absorbance precision at 1 s sampling rate. For N_2O this yields a MDND calculated from 3 ppb at 60 Torr. For CH_4 the MDND was estimated from the Allan variance after 200 s: 0.7 ppb at 50 Torr (Ref. 1).

[81]Figure 5 in Ref. 1 implies a minimum absorbance of 4×10^{-5} for a 1 Hz sampling rate at 56 m path length which yields the (short term) NEA from Eqs. (18) and (19) (without $\sqrt{2}$). The MDND follows from 35.5 Torr (Fig. 3) and the Allan variance minimum of 0.06 ppb.

[82]The MDND was calculated for 48 Torr and 1 s averaging time (Fig. 3) by means of the given NEAs, i.e., 0.12 and 0.26 ppb for the LN and TE cooled detectors, respectively (Ref. 39).

[83]The MDNDs follow from 34 and 14 ppb for CH_4 and N_2O at atmospheric pressure, respectively. The NEA was estimated from the noise of 0.4 μV and the calibration factor of 715 $V/W\ cm^{-1}$ scaled with the output power of 8 mW (Ref. 41).

[84]The MDND follows from 4 ppb at 50 Torr for a 3 s lock-in time constant. The normalized NEA was scaled with the output power of 19 mW (Ref. 42).

[85]The MDND was calculated with 0.1 ppb at 770 Torr after 100 s (Allan variance plot). The normalized NEA was scaled with the output power of 6.6 mW (Ref. 40).